Effect of multiple cationic substitutions on structure and magnetism of honeycomb-layered hexagonal tellurates $Na_2M_2TeO_6$ (M = Co, Ni, Cu, Zn)

Vladimir B. Nalbandyan[1,*], Igor L. Shukaev,[1] Maria A. Evstigneeva[1], Alexander N. Vasiliev[2], Tatyana M. Vasilchikova[2]

[1]*Southern Federal University, Rostov-on-Don 344090, Russia*

[2]*Lomonosov Moscow State University, Moscow 119991, Russia*

Abstract

Hexagonal layered $Na_2T_2TeO_6$ (T = $Co_{1/3}Ni_{1/3}Cu_{1/3}$) and $Na_2Z_2TeO_6$ (Z = $Co_{1/4}Ni_{1/4}Cu_{1/4}Zn_{1/4}$) have been prepared by solid-state reactions. According to the X-ray Rietveld refinement, $Na_2Z_2TeO_6$ is isostructural with its honeycomb-ordered constituents $Na_2M_2TeO_6$ (M = Co, Zn), space group $P6_322$. For $Na_2T_2TeO_6$, however, only subcell (ignoring T/Te ordering) could be successfully refined despite presence of weak superstructure reflection. This is attributed to intergrowth of two packing modes with similar lattice parameters: $P6_3/mcm$ (characteristic of $Na_2Ni_2TeO_6$) and $P6_322$. According to magnetic susceptibility and heat capacity measurements, both materials undergo antiferromagnetic ordering at low temperatures with negative Weiss temperatures of −38 and −26 K for the T- and Z-compositions, respectively. The Néel point of $Na_2T_2TeO_6$, 16.9 K, is considerably lower than those of its Ni and Co constituents (both being about 27 K), in contrast to the sister system, monoclinic $Na_3T_2SbO_6$, where T_N is intermediate between those of Ni and Co constituents. Further lowering of the Néel point in $Na_2Z_2TeO_6$, 8.6 K, is attributed to the diamagnetic dilution with Zn^{2+}.

1. Introduction

Layered mixed oxides with honeycomb ordering of divalent 3d cations, $A_3M_2XO_6$ (A = Li, Na; M^{2+} = Mn, Fe, Co, Ni; X = Sb, Bi) and $A_2M_2TeO_6$ (A = Na, K; M^{2+} = Co, Ni) attract much attention due to the diversity of their ground states and proximity to Kitaev's physics. Compounds with M^{2+} = Cu formally belong to the same multitude but the Jahn-Teller effect inherent to d^9 cation leads to strong distortion and results in quite different Cu-Cu distances (one short and two long). Thus, magnetic honeycomb is cut into spin dimers and alternating spin chains.[1,2]

Numerous works were devoted to individual compounds of these families, with fewer studies on their binary solid solutions.[3-11] Naturally, dilution of Mn^{2+}, Fe^{2+}, Co^{2+} or Ni^{2+} ions with diamagnetic Mg^{2+} or Zn^{2+} ions shifts the Néel temperature downward and, at high enough concentration, suppresses the antiferromagnetic (AFM) order.[3-5,7-11] The same was observed at

*Corresponding author. E-mail: vbn@sfedu.ru

Cu^{2+} substitution for Ni^{2+} in $Li_3Ni_2BiO_6$[9] and $Na_3Ni_2SbO_6$[5]. Similarly, the spin gap behavior of $Na_3Cu_2SbO_6$ is suppressed by Mg^{2+}, Zn^{2+} or Ni^{2+} doping.[5] However, the AFM state persists at least up to 50% diamagnetic substitution in $Na_2Co_{2-x}Zn_xTeO_6$,[4,11] $Li_3CoMSbO_6$ (M = Mg, Zn),[7] $Na_3(MnZn)SbO_6$ and $Na_3(FeM)SbO_6$ (M = Mg, Zn).[8] In $Na_2Co_{2-x}Ni_xTeO_6$, Néel temperature varies almost linearly from 26 K (x = 0) to 34 K (x = 1).[4] $Li_3NiCoSbO_6$ shows slightly reduced T_N of 10 K,[7] compared to those of $Li_3Ni_2SbO_6$ (15 K[12]) and $Li_3Co_2SbO_6$ (14 K[13] or 10 K[14]).

Studies on rapidly growing class of "high-entropy" (HE) or "compositionally complex" magnetic oxides[15-32] have shown that their properties usually are not mere linear combinations of the properties of components. Although a large number of these oxides are antiferromagnets, other ground states are realized in some compounds. In particular, competing exchange interactions between several magnetically active ions may lead to spin-glass-type behavior instead of a long-range magnetic order.[15-21] Iron-containing spinels[22] and magnetoplumbite[23,24] order ferromagnetically, whereas bixbyite $Gd_{0.4}Tb_{0.4}Dy_{0.4}Ho_{0.4}Er_{0.4}O_3$[25] and orthorhombic perovskite $(Gd_{0.2}Nd_{0.2}\ La_{0.2}Sm_{0.2}Y_{0.2})CoO_3$[26] stay paramagnetic down to 5 and 3 K, respectively. This diversity of ground states is apparently due to a large number of competing exchange interactions due to extremely high chemical disorder in HE oxides.

To our knowledge, the only study of magnetism in "compositionally complex" (with more than two mixed divalent cations) representatives of the above honeycomb-layered families was our work on monoclinic $A_3T_2SbO_6$ where A = Li or Na and $T = Co_{1/3}Ni_{1/3}Cu_{1/3}$.[19] There, owing to dilution with non-Jahn-Teller ions, the distortion of the honeycomb layers is suppressed, M^{2+}-M^{2+} distances are more uniform and Cu^{2+} ions are involved into the honeycomb order (and the same is observed in the present work with $Na_2T_2TeO_6$ and $Na_2(Co_{1/2}Ni_{1/2}Cu_{1/2}Zn_{1/2})TeO_6$). $Na_3T_2SbO_6$ undergoes AFM ordering at 10 K whereas $Li_3T_2SbO_6$ shows pronounced spin-cluster effect without long-range magnetic ordering.

The aims of the present work were:

(i) to study magnetic effects in a different multicomponent honeycomb structure, hexagonal $Na_2T_2TeO_6$;

(ii) to investigate the effect of a diamagnetic dilution in $Na_2Z_2TeO_6$ ($Z = Co_{1/4}Ni_{1/4}Cu_{1/4}Zn_{1/4}$).

Of the four constituent simple tellurates $Na_2M_2TeO_6$, only those with M = Co and Zn are isostructural (space group $P6_322$). $Na_2Ni_2TeO_6$ has very similar lattice parameters but a different packing type (space group $P6_3/mcm$).[33] Both these structure types are superstructures of the well-known P2 type (space group $P6_3/mmc$), that is, double-layered packing with prismatic coordination of the interlayer sodium ions. The compound with $M = Cu$[34] is a monoclinic superstructure of the O3 type (α-$NaFeO_2$), isostructural with antimonates mentioned above. In the

present work, equimolar combinations of three or four of the above tellurates resulted in two single phases with different packing types.

2. Experimental

2.1. Sample preparation and characterization

Details of starting materials, solid-state preparations, hazards and precautions are reported in the Supporting Information File. Powder X-ray diffraction (XRD) was performed using an ARL X'TRA diffractometer with copper anode and solid-state Si(Li) detector. To suppress grain orientation, typical of the layered phases, powders were mixed with an amorphous low-attenuating medium (instant coffee or beryllium basic carbonate). The Rietveld profile refinements were done using the GSAS-II suite.[35]

2.2. Physical measurements

Both DC and AC susceptibility χ and specific heat C_p of pressed pellets of 3 mg were studied using relevant options of "Quantum Design" Physical Properties Measurements System PPMS-9T. The magnetization isotherms were measured using Quantum Design SQUID magnetometer.

3. Results and discussion

3.1. Crystal structures

XRD patterns of $Na_2T_2TeO_6$ and $Na_2Z_2TeO_6$ (**Fig. 1**) have been completely indexed as hexagonal P2-type superstructures with lattice parameters very similar to those of the monocation $Na_2M_2TeO_6$ (M = Co, Ni, Zn, Mg)[33] but different systematic absences, although superstructure reflections arising from *T*/Te or *Z*/T ordering are abnormally weak. Formally, this may be explained by partially inverted *T*/Te or *Z*/T occupancies. However, random mixing of components with so different oxidation states (2+ and 6+) is hardly possible, and most probable explanation is faulted packing of completely ordered layers, as demonstrated for $Na_3Ni_2SbO_6$ by ^{23}Na NMR, HRTEM and SAED.[36,37]

For $Na_2T_2TeO_6$, there are no 00*l* and h0*l* reflections with odd *l*. The highest symmetry space group obeying these rules is $P6_3/mcm$, just as for $Na_2Ni_2TeO_6$.[33] For $Na_2Z_2TeO_6$, only the first of these rules is valid, whereas reflections 101, 103, 201, and 303 are clearly visible. Then, the highest symmetry space group is $P6_322$, just as for $Na_2M_2TeO_6$ (M = Co, Zn, Mg).[33] Thus, the crystal structures of $Na_2Ni_2TeO_6$ and $Na_2Zn_2TeO_6$ were taken as starting models for $Na_2T_2TeO_6$ and $Na_2Z_2TeO_6$, respectively. The main results are shown in **Fig. 1** and **Tables S1**, **S2,** and **1**.

For $Na_2Z_2TeO_6$, the refinement converged to reasonably low residuals (**Table S1**) and average *Z*-O and Te-O bond distances in agreement with sums of corresponding crystallographic radii[38] (**Table 1**). To account for weakened superlattice effects, partial *Z*/T site inversion was formally introduced, as in many preceding works, e.g.[19,37] Due to the very similar scattering factors

of all four transition metals, only Ni/Te inversion was implied for simplicity. Of course, the resulting *Z*/T occupancies (**Table S2**) are only formal fitting parameters and do not imply actual site disorder. There are three prismatic sodium sites in $Na_2Zn_2TeO_6$ with occupancies of 0.280, 0.043, and 0.535[33] or 0.5, 0, 0.25[39], respectively. During our refinement of $Na_2Z_2TeO_6$, the occupancy of Na2 tended to be slightly negative. Therefore, it was fixed at zero but we did not change site numbers to facilitate comparison with the prototype.

For $Na_2T_2TeO_6$, however, analogous refinement did not go well and reliable results could not be obtained due to the instability of convergence process. We attribute this fact to additional stacking disorder, probably intergrowth of $P6_3/mcm$ and $P6_322$ packing modes, manifested also in especial broadening and weakness of the superstructure reflections. Therefore, only substructure might be refined ignoring *T*/Te honeycomb ordering, although, as noticed above, each individual layer is believed to be completely ordered.

Elevated Na-O distances and elevated displacement parameters of sodium ions in both phases are due to low occupancies,[38] high mobility and local disorder of sodium ions because of the asymmetric Na^+-Na^+ repulsion in adjacent partially occupied prisms.[33]

Table 1. Main interatomic distances (Å) in $Na_2Z_2TeO_6$ (true superstructure) and $Na_2T_2TeO_6$ (refined as a substructure) in comparison with corresponding sums of (averaged) ionic radii.

$Na_2Z_2TeO_6$		Average	ΣR[38]
(Te,*Z*)-O	1.953(9)×6		1.976
(*Z*1,Te)-O	2.092(6)×6		2.102
(*Z*2,Te)-O	2.071(9)×6		2.102
Na1-O	2.437(9)×2	2.492	2.41
	2.510(20)×2		
	2.528(11)×2		
Na3-O	2.469(32)×3	2.469	2.41
	2.470(34)×3		
$Na_2T_2TeO_6$			
(*T*,Te)-O	2.033(3)×6		2.058
Na1-O	2.482(5)×6		2.41
Na2-O	2.482(5)×6		2.41

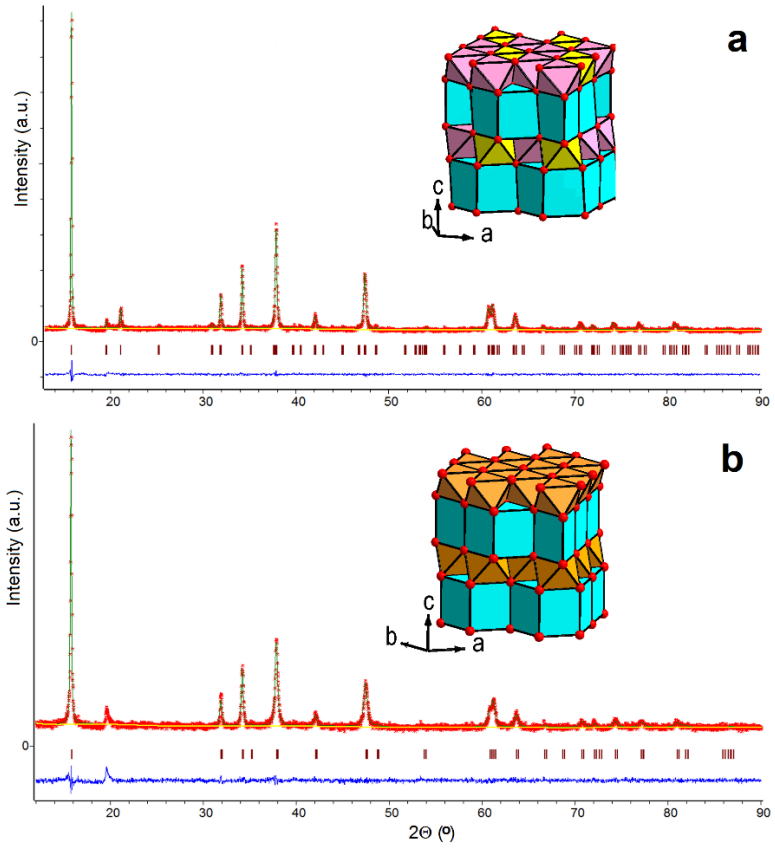

Figure 1. Results of the Rietveld refinements and polyhedral presentation of crystal structures of (a) $Na_2Z_2TeO_6$ (true superstructure) and (b) $Na_2T_2TeO_6$ (refined as a substructure, ignoring superstructure reflections). Red crosses: experimental points; green line: calculated profile; blue line: difference profile; vertical bars: Bragg positions; red balls: oxygen; blue prisms: NaO_6; pink octahedra: ZO_6; yellow octahedra: TeO_6; orange octahedra: (T, Te)O_6.

3.2. Magnetic properties

Temperature dependences of the magnetic susceptibility χ at $\mu_0 H$ = 0.1 T for $Na_2T_2TeO_6$ and $Na_2Z_2TeO_6$ are shown in **Fig. 2**. The χ(T) curve for $Na_2T_2TeO_6$ demonstrates a sharp peak at T_N = 16.9 K, which points to the establishment of long-range antiferromagnetic order. For $Na_2Z_2TeO_6$, the magnetic susceptibility recorded in the field-cooled (FC) regime increases with decreasing temperature and evidences a kink at the T_N = 8.6 K. The χ(T) curves for both compounds can be fitted by the Curie-Weiss law in the paramagnetic region:

$$\chi = \chi_0 + \frac{C}{T - \Theta}, \quad (1)$$

where χ_0 is the temperature-independent contribution, C is the Curie constant, Θ is the Weiss temperature. To independently estimate χ_0 value, we summed up Pascal's constants[40] for the diamagnetic contributions of ions in $Na_2T_2TeO_6$ and $Na_2Z_2TeO_6$ and the resulting values were -$1.21 \cdot 10^{-4}$ emu/mol and -$1.22 \cdot 10^{-4}$ emu/mol, respectively. The negative Weiss temperatures Θ =

−38 ± 1 K and –26 ± 1 K for $Na_2T_2TeO_6$ and $Na_2Z_2TeO_6$, respectively, indicate the dominant antiferromagnetic interaction in the studied compounds.

The Curie constant obtained from this approximation can be used to determine the effective magnetic moment:

$$C = \frac{N_A}{3k_B}\mu_{eff}^2 \quad (2)$$

On the other hand, a theoretical estimation of the effective magnetic moment can be obtained by the equation:

$$\mu_{th} = \sqrt{\sum_i n_i g_i^2 S_i(S_i+1)}\,\mu_B \quad (3)$$

where *n* is the number of magnetic centers, *g* denotes the g-factor, and *S* is the spin for each of the ions of the magnetic subsystem. The theoretical values turned out to be slightly lower than the experimentally obtained ones, as shown in **Table 2**. The deviation of the experimental effective moments from the numerical estimations can be explained by the uncertainty in the value of the effective g-factor for the Co^{2+} ion.

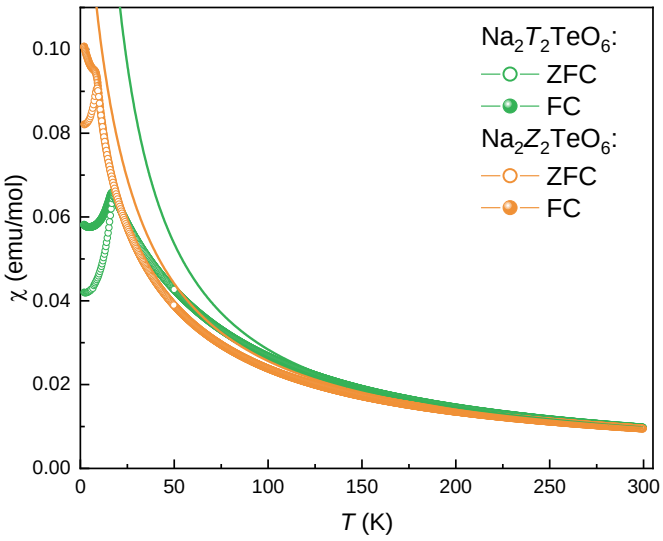

Figure 2. Temperature dependences of magnetic susceptibility $\chi = M/B$ at $\mu_0 H$ = 0.1 T for $Na_2T_2TeO_6$ and $Na_2Z_2TeO_6$ recorded in zero-field-cooled ZFC (filled symbols) and field-cooled FC (open symbols). The solid lines are the fits by the Curie–Weiss law.

Table 2. The main parameters of the magnetic subsystem in $Na_2T_2TeO_6$ and $Na_2Z_2TeO_6$

	T_N	χ_0	Θ	μ_{th}	μ_{eff}
$Na_2T_2TeO_6$	16.9	$1.21\cdot10^{-4}$	−38 ± 1	$4.70\mu_B$	$4.93\mu_B$
$Na_2Z_2TeO_6$	8.6	$1.22\cdot10^{-4}$	−26 ± 1	$4.07\mu_B$	$4.97\mu_B$

Under an external magnetic field $\mu_0 H$ = 9 T, the anomaly corresponding to the Néel temperature for $Na_2T_2TeO_6$ is blurred, and its position shifts to lower temperatures side (**Fig. S1a**). In case of $Na_2Z_2TeO_6$, the anomaly at T_N = 8.6 K is completely suppressed by the external magnetic field 9 T, as shown in **Fig. S1b**.

Full magnetization curves for $Na_2T_2TeO_6$ and $Na_2Z_2TeO_6$ were taken at T = 2 K in the magnetic field range $-9 < H < 9$ T (**Fig. 3**). The field dependence of magnetization $M(H)$ for $Na_2T_2TeO_6$ does not show hysteresis. The change in the slope of the M/H curve is observed at $\mu_0 H_{SF}$ = 4 T, which can be ascribed to a spin-flop transition expected for an ordered AFM state (inset in **Fig. 3**). It should be noted that even at $\mu_0 H$ = 9 T, the magnetization is far from the saturation value, $M_{sat} = (n_{Cu}g_{Cu}S_{Cu} + n_{Co}g_{Co}S_{Co} + n_{Ni}g_{Ni}S_{Ni})\mu_B = 4.5\mu_B$. In case of $Na_2Z_2TeO_6$, the main difference from the data for the Zn-free analogue ($Na_2T_2TeO_6$) is the presence of a small but noticeable hysteresis in moderate magnetic fields. This may indicate the presence of weak ferro- or ferrimagnetic interactions. No spin-flop-type features were observed in this compound.

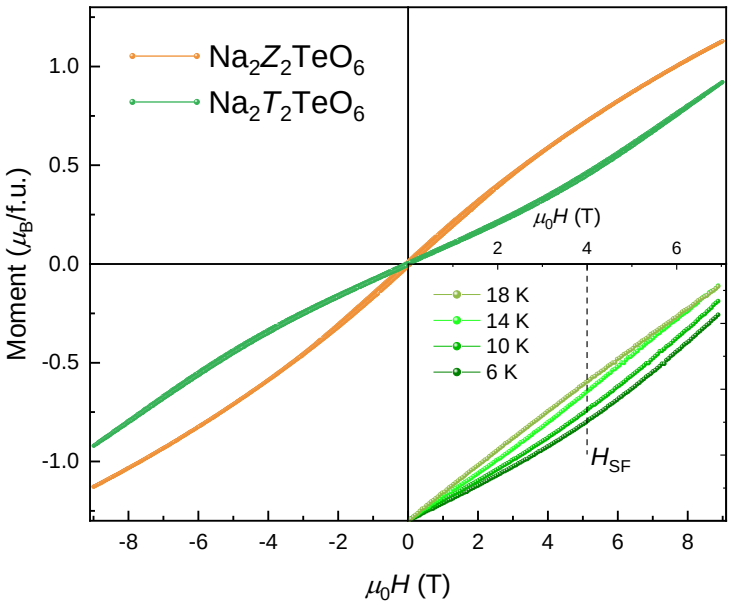

Figure 3. Full magnetization isotherms $M(H)$ at T = 2 K for $Na_2T_2TeO_6$ and $Na_2Z_2TeO_6$. Inset: $M(H)$ curves for $Na_2M_2TeO_6$ at various temperatures.

Additional AC susceptibility study was carried out for $Na_2Z_2TeO_6$ (**Fig. S2**). The real part χ' evidences the anomaly at T = 8.5 K, which corresponded to the kink temperature in the static magnetic susceptibility. The position of this anomaly does not depend on frequency, which rules out the spin-glass processes.

The specific heat data $C_p(T)$ in zero magnetic field for $Na_2T_2TeO_6$ and $Na_2Z_2TeO_6$ were found to be in a good agreement with the magnetization data, showing clear anomalies at the magnetic phase transitions (**Fig. 4**). In order to clarify the nature of the magnetic phase transition and evaluate its effect on the specific heat and entropy, the temperature dependence of specific heat $C_p(T)$ was also measured for their nonmagnetic analogue $Na_2Zn_2TeO_6$. The standard scaling procedure[41] was applied to the C_p data for both $Na_2T_2TeO_6$ and $Na_2Z_2TeO_6$ to estimate the lattice phonon contribution $C_{ph}(T)$, which allows to define the value of magnetic entropy $S_m(T)$.

The change in entropy with increasing temperature is shown in the inset of **Fig. 4**. It can be seen that the magnetic entropy saturates at $T \sim 80$ K for $Na_2T_2TeO_6$ and ~60 K for $Na_2Z_2TeO_6$. The values of magnetic entropy are noticeably smaller than expected from the mean field theory[42]

$$\sum_i n_i \ln(2S_i + 1) \quad (4)$$

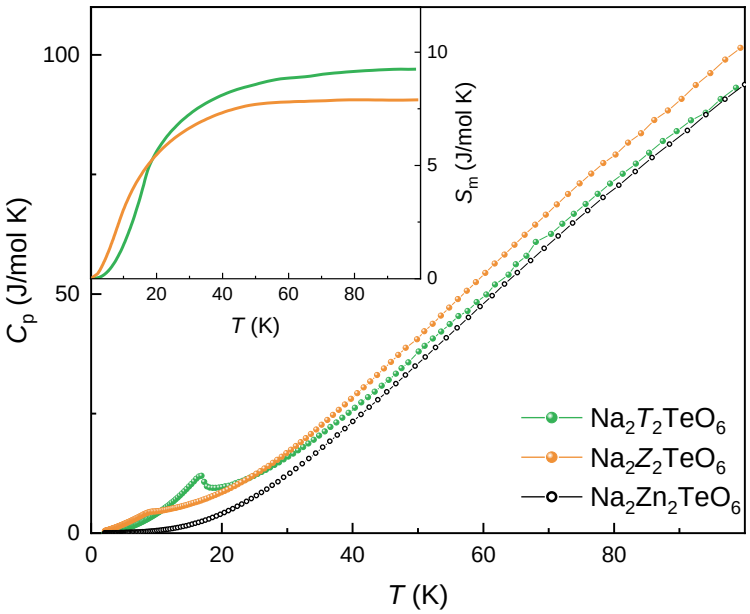

Figure 4. The specific heat $C_p(T)$ for $Na_2T_2TeO_6$ and $Na_2Z_2TeO_6$ (filled symbols) and their nonmagnetic analog $Na_2Zn_2TeO_6$ (open circles) at $\mu_0H = 0$ T. Inset: magnetic entropy S_m(T).

By combining magnetization isotherm data (inset in **Fig. 3**) and specific heat data under external magnetic fields (**Fig. S3**), a magnetic phase diagram was obtained for $Na_2T_2TeO_6$. In zero magnetic field, the paramagnetic phase was realized at temperatures higher than 17 K. Application of a magnetic field shifts downward the Néel temperature (**Fig. 5**). It follows from this diagram that the ground state of $Na_2T_2TeO_6$ is antiferromagnetic (AFM1). Under magnetic field this compound experiences transition into the spin-flop phase (AFM2).

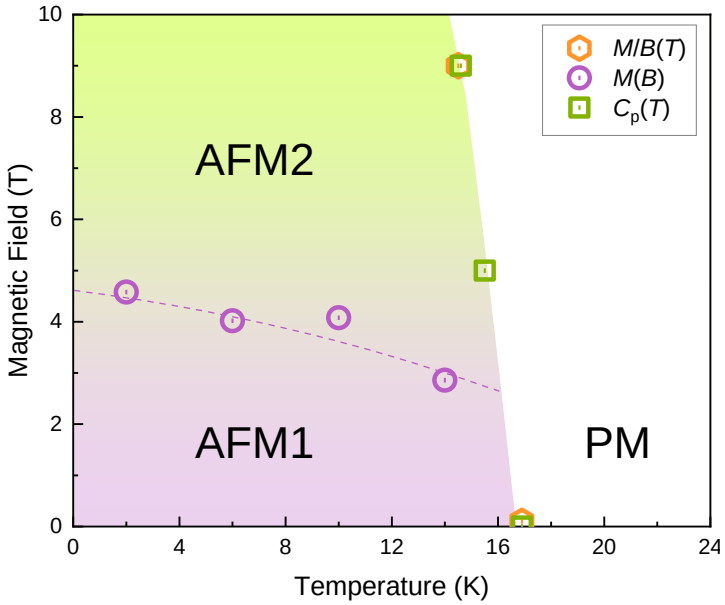

Figure 5. The magnetic phase diagram for $Na_2T_2TeO_6$.

Conclusions

$Na_2Z_2TeO_6$ and $Na_2T_2TeO_6$ are different honeycomb-type superstructures of the well-known layered P2 type. The former is isostructural with $Na_2M_2TeO_6$ (M = Co, Zn, Mg). For the latter, $Na_2Ni_2TeO_6$ type or its intergrowth with $Na_2Zn_2TeO_6$ type is supposed. Both $Na_2T_2TeO_6$ and $Na_2Z_2TeO_6$ order antiferromagnetically at T_N = 16.9 and 8.6 K, respectively. The Weiss temperatures are negative, $\Theta = -38 \pm 1$ K and -26 ± 1 K, which highlights the antiferromagnetic correlations in the high-temperature paramagnetic region. Lower values of both T_N and Weiss temperature Θ for $Na_2Z_2TeO_6$ compared to $Na_2T_2TeO_6$ indicate a weakening of exchange interactions upon non-magnetic dilution with zinc ions.

ASSOCIATED CONTENT

Supporting Information

The Supporting Information is available at the end of this file.

Starting materials; sample preparation; hazards and precautions; details of structure refinement; atomic coordinates, site occupancy factors and displacement parameters; temperature dependencies of magnetic susceptibility and specific heat under various magnetic fields; temperature dependences of the real χ' part of AC magnetic susceptibility χ_{AC} for $Na_2Z_2TeO_6$ at various frequencies.

Accession Codes

Deposition Numbers 2401832 and 2401833 contain the supplementary crystallographic data for this paper. These data can be obtained free of charge via the joint Cambridge Crystallographic

Data Centre (CCDC) and Fachinformationszentrum Karlsruhe Access Structures service. www.ccdc.cam.ac.uk/data_request/cif

ACKNOWLEDGMENT

The work was supported by the Russian Science Foundation under the grant 23-23-00520.

References

(1) Schmitt, M.; Janson, O.; Golbs, S.; Schmidt, M.; Schnelle, W.; Richter, J.; Rosner, H. Microscopic magnetic modeling for the S = 1/2 alternating chain compounds $Na_3Cu_2SbO_6$ and $Na_2Cu_2TeO_6$, *Phys. Rev. B.* **2014**, *89*, 174403. DOI: 10.1103/PhysRevB.89.174403

(2) Bhattacharyya, A.; Bhowmik, T.K.; Adroja, D.T.; Rahaman, B.; Kar, S.; Das, S.; Saha-Dasgupta, T.; Biswas, P.K.; Sinha, T.P.; Ewings, R.A.; Khalyavin, D.D.; Strydom A.M. Dynamic spin fluctuations in the frustrated spin chain compound $Li_3Cu_2SbO_6$. *Phys. Rev. B.* **2021**, *103*, 174423. DOI: 10.1103/PhysRevB.103.174423

(3) Berthelot, R.; Schmidt, W.; Muir, S.; Eilertsen, J.; Etienne, L.; Sleight, A.W.; Subramanian, M. A. New Layered Compounds with Honeycomb Ordering: $Li_3Ni_2BiO_6$, $Li_3NiM'BiO_6$ (M′ = Mg, Cu, Zn), and the Delafossite $Ag_3Ni_2BiO_6$. *Inorg. Chem.* **2012,** *51*, 5377−5385. DOI: 10.1021/ic300351t

(4) Berthelot, R.; Schmidt, W.; Sleight, A.W.; Subramanian, M.A. Studies on solid solutions based on layered honeycomb-ordered phases P2-$Na_2M_2TeO_6$ (M=Co, Ni, Zn). *J. Solid State Chem.* **2012**, *196*, 225-231. DOI: 10.1016/j.jssc.2012.06.022

(5) Schmidt, W; Berthelot, R.; Sleight, A.W.; Subramanian, M.A. Solid solution studies of layered honeycomb-ordered phases O3-$Na_3M_2SbO_6$ (M = Cu, Mg, Ni, Zn). *J. Solid State Chem.* **2013**, *201*, 178-185. DOI: 10.1016/j.jssc.2013.02.035

(6) Yadav, D.K.; Sethi, A.; Shalu; Uma, S. New series of honeycomb ordered oxides, $Na_3M_2SbO_6$ (M(II) = Mn, Fe, (Mn, Fe), (Mn, Co)): synthesis, structure and magnetic properties. *Dalton Trans.* **2019**, *48*, 8955-8965. DOI: 10.1039/c9dt01194c

(7) Pal, S.; Yadav, D.K.; Uma, S. Insights into the honeycomb ordered $Li_3(MnM)SbO_6$ (M(II) = Co, Ni, Zn, Mg) and $Li_3(CoM')SbO_6$ (M′(II) = Ni, Zn, Mg) oxides. *Solid State Sci.* **2022**, *128*, 106894. DOI: 10.1016/j.solidstatesciences.2022.106894

(8) Yadav, D.K.; Sethi, A.; Uma, S. Investigation of the structure, optical and magnetic properties of the honeycomb layered $Na_3(MnIIM)SbO_6$ (M (II) = Fe, Co, Ni, Zn, Mg) and $Na_3(FeIIM')SbO_6$ (M′ (II) = Co, Ni, Zn, Mg) oxides. *Mater. Today Commun.* **2022**, *30*, 103012. DOI: 10.1016/j.mtcomm.2021.103012

(9) Kumar, R; Sundaresan, A. Spin-glass behavior in Li3NiCuBiO6: a two-dimensional distorted honeycomb-lattice. *J. Phys.: Condens. Matter* **2022**, *34*, 415803. DOI: 10.1088/1361-648X/ac86b2

(10) Fu, Z.; Xu, R.; Chen, Y.; Bao, S.; Du, H.; Min, J.; Zheng, S.; Zhang, Y.; Liu, M.; Wang, X.; Li, H.; Zhong, R.; Luo, H.; Liu, J.-M.; Ma, Z.; Wen, J. Signatures of a gapless quantum spin liquid in the Kitaev material $Na_3Co_{2-x}Zn_xSbO_6$, *Phys. Rev. B,* **2023**, *107*, 165143. DOI: 10.1103/PhysRevB.107.165143

(11) Fu, Z.; Xu, R.; Bao, S.; Shangguan, Y.; Liu, X.; Lu, Z.; Chen, Y.; Zheng, S.; Zhang, Y.; Liu, M.; Wang, X.; Li, H.; Luo, H.; Liu, J.-M.; Ma, Z.; Wen, J. Suppression of the antiferromagnetic order by Zn doping in a possible Kitaev material $Na_2Co_2TeO_6$. *Phys. Rev. Mater.* **2023**, *7*, 014407. DOI: 10.1103/PhysRevMaterials.7.014407

(12) Zvereva, E.A.; Evstigneeva, M.A.; Nalbandyan, V. B.; Savelieva, O.A.; Ibragimov, S.A.; Volkova, O.S.; Medvedeva, L.I.; Vasiliev, A.N.; Klingeler, R.; Buechner, B. Monoclinic honeycomb-layered compound $Li_3Ni_2SbO_6$: preparation, crystal structure and magnetic properties. *Dalton Trans.* **2012**, *41*, 572-580. DOI: 10.1039/c1dt11322d

(13) Brown, A.J.; Xia, Q.; Avdeev, M.; Kennedy, B.J.; Ling, C.D. Synthesis-controlled polymorphism and magnetic and electrochemical properties of $Li_3Co_2SbO_6$. Inorg. Chem. **2019**, 58, 13881-13891. DOI: 10.1021/acs.inorgchem.9b01708

(14) Stratan, M. I.; Shukaev, I. L.; Vasilchikova, T. M.; Vasiliev, A.N.; Korshunov, A. N.; Kurbakov, A. I.; Nalbandyan, V. B.; Zvereva, E.A. Synthesis, structure and magnetic properties of honeycomb-layered $Li_3Co_2SbO_6$ with new data on its sodium precursor, $Na_3Co_2SbO_6$. *New J. Chem.* **2019,** *43*, 13545−13353. DOI: 10.1039/c9nj03627j

(15) Sarkar, A.; Kruk, R.; Hahn, H. Magnetic properties of high entropy oxides. *Dalton Trans.* **2021**, *50*, 1973-1982. DOI: 10.1039/D0DT04154H

(16) Kotsonis, G.N.; Almishal, S.S.I.; dos Santos Vieira, F.M.; Crespi, V.H.; Dabo, I.; Rost, C.M.; Maria, J.-P. High-entropy oxides: Harnessing crystalline disorder for emergent functionality. *J. Am. Ceram. Soc.* **2023**, *106*, 5587-5611. DOI: 10.1111/jace.19252

(17) Jimenez-Segura, M. P.; Takayama, T.; Bérardan, D.; Hoser, A.; Reehuis, M.; Takagi, H.; Dragoe, N. Long-range magnetic ordering in rocksalt-type high-entropy oxides. *Appl. Phys. Lett.*, **2019**, 114, 122401. DOI: 10.1063/1.5091787

(18) Kinsler-Fedon, C.; Zheng, Q.; Huang, Q.; Choi, E. S.; Yan, J.; Zhou, H.; Mandrus, D.; Keppens, V. Synthesis, characterization, and single-crystal growth of a high-entropy rare-earth pyrochlore oxide. Phys. Rev. Mater., 2020, 4, 104411. DOI: 10.1103/PhysRevMaterials.4.104411

(19) Nalbandyan, V.B.; Vasilchikova, T.M.; Evstigneeva, M.A.; Vasiliev, A.N.; Shukaev, I.L. Spin-Cluster Glassy and Long-Range Ordered Magnetic States in Honeycomb-Layered

Compositionally Complex Oxides $Na_{3-x}Li_xT_2SbO_6$ (T = $Cu_{1/3}Ni_{1/3}Co_{1/3}$). *Inorg. Chem.* **2024,** *63*, 5012-5019. DOI: 10.1021/acs.inorgchem.3c04436

(20) Nalbandyan, V. B.; Evstigneeva, M. A.; Bazhan, R. V.; Vasiliev, A. N.; Bulgakov, A. N.; Vasilchikova, T.M. Ionic substitutions in the Cu_3TeO_6 structure type and magnetic properties of "medium entropy" $Cu_{3/2}Mn_{1/2}Co_{1/2}Fe_{1/2}SbO_6$. *J. Solid State Chem.* 2024, **340** 125013. DOI: 10.1016/j.jssc.2024.125013

(21) Clulow, R.; Pramanik, P.; Stolpe, A.; Joshi, D.C.; Mathieu, R.; Henry, P.F.; Sahlberg, M. Phase Stability and Magnetic Properties of Compositionally Complex n = 2 Ruddlesden−Popper Perovskites. *Inorg. Chem.* **2024**, *63*, 6616−6625. DOI: 10.1021/acs.inorgchem.3c04277

(22) Musicó, B.; Wright, Q.; Ward, T. Z.; Grutter, A.; Arenholz, E.; Gilbert, D.; Mandrus, D.; Keppens, V. Tunable magnetic ordering through cation selection in entropic spinel oxides. *Phys. Rev. Mater.*, **2019**, 3, 104416. DOI: 10.1103/PhysRevMaterials.3.104416

(23) Vinnik, D. A.; Trukhanov, A. V.; Podgornov, F. V.; Trofimov, E. A.; Zhivulin, V. E.; Starikov, A. Y.; Zaitseva, O. V.; Gudkova, S. A.; Kirsanova, A. A.; Taskaev, S. V.; Uchaev, D. A.; Trukhanov, S. V.; Almessiere, M. A.; Slimani, Y.; Baykal, A. Correlation between entropy state, crystal structure, magnetic and electrical properties in M-type Ba-hexaferrites. *J. Eur. Ceram. Soc.*, **2020**, 40, 4022–4028. DOI: 10.1016/j.jeurceramsoc.2020.04.036

(24) Zhivulin, V.E.; Trofimov, E.A.; Zaitseva, O.V.; Sherstyuk, D.P.; Cherkasova, N.A.; Taskaev, S.V.; Vinnik, D.A.; Alekhina, Yu.A.; Perov, N.S.; Tishkevich, D.I.; Zubar, T.I.; Trukhanov, A.V.; Trukhanov, S.V. Effect of configurational entropy on phase formation, structure, and magnetic properties of deeply substituted strontium hexaferrites. *Ceram. Intern.*, **2023**, *49*, 1069–1084. DOI: 10.1016/j.ceramint.2022.09.082

(25 Tseng, K.; Yang, Q.; McCormack, S. J.; Kriven, W. M. High-entropy, phase-constrained, lanthanide sesquioxide. *J. Am. Ceram. Soc.*, **2020**, 103, 569–576. 10.1111/jace.16689

(26) Krawczyk, P. A.; Jurczyszyn, M.; Pawlak, J.; Salamon, W.; Baran, P.; Kmita, A.; Gondek, Ł.; Sikora, M.; Kapusta, C.; Strączek, T.; Wyrwa, J.; Żywczak, A. High-Entropy Perovskites as Multifunctional Metal Oxide Semiconductors: Synthesis and Characterization of $(Gd_{0.2}Nd_{0.2}La_{0.2}Sm_{0.2}Y_{0.2})CoO_3$. *ACS Appl. Electron. Mater.*, **2020**, 2, 3211–3220. DOI: 10.1021/acsaelm.0c00559

(27) Kirsch, A.; Bøjesen, E.D.; Lefeld, N.; Larsen, R.; Mathiesen, J.K.; Skjærvø, S.L.; Pittkowski, R.K.; Sheptyakov, D.; Jensen, K.M.Ø. High-Entropy Oxides in the Mullite-Type Structure. *Chem. Mater.* **2023**, *35*, 8664−8674. DOI: 10.1021/acs.chemmater.3c01830

(28) Katzbaer, R.R.; Vincent, W.M.; Mao, Z.; Schaak, R.E. Synthesis and Magnetic, Optical, and Electrocatalytic Properties of High-Entropy Mixed-Metal Tungsten and Molybdenum Oxides. *Inorg. Chem.* **2023**, *62*, 7843−7852. DOI: 10.1021/acs.inorgchem.3c00541

(29) Nalbandyan, V.B.; Vasilchikova, T.M.; Zakharov, K.V.; Vasiliev, A.N.; Evstigneeva, M.A.; Guda, A.A. Preparation and Properties of a High-Entropy Wolframite-Type Antiferromagnet, $(Mn_{0.2}Co_{0.2}Ni_{0.2}Cu_{0.2}Cd_{0.2})WO_4$. *Inorg. Chem.* **2024**, *63*, 10099–10102. DOI: 10.1021/acs.inorgchem.3c04430

(30) Yan, J.; Kumar, A.; Chi, M.; Brahlek, M.; Ward, T.Z.; McGuire, M.A. Orbital degree of freedom in high entropy oxides. *Phys. Rev. Mater.*, **2024,** *8*, 024404. DOI: 10.1103/PhysRevMaterials.8.024404

(31) Martin, C.; Bolletta, J.P.; Maignan, A. Compositional Complexity as a Design Principle for Stabilizing Magnetization Reversal in Corundum-Derived $A_4Nb_2O_9$ Phases. *Chem. Mater.* **2024**, *36*, 1753−1762. DOI: 10.1021/acs.chemmater.3c03181

(32) Nalbandyan, V. B.; Zakharov, K. V,; Evstigneeva, M. A.; Vasiliev, A. N.; Sheptun, I. G.; Shvanskaya, L. V.; Vasilchikova, T. M., Preparation and Characterization of a High-Entropy Magnet, $(Mg, Mn, Co, Ni, Cu)_3TeO_6$, *Inorg. Chem*. **2024**, DOI: 10.1021/acs.inorgchem.4c02809

(33) Evstigneeva, M.A.; Nalbandyan, V.B.; Petrenko, A.A.; Medvedev, B.S.; Kataev, A.A. A new family of fast sodium ion conductors: $Na_2M_2TeO_6$ (M = Ni, Co, Zn, Mg). *Chem. Mater.* **2011**, *23*, 1174–1181. DOI: 10.1021/cm102629g.

(34) Xu, J.; Assoud, A.; Soheilnia, N.; Derakhshan, S.; Cuthbert, H.L.; Greedan, J.E.; Whangbo, M.H.; Kleinke, H. Synthesis, structure, and magnetic properties of the layered copper(II) oxide $Na_2Cu_2TeO_6$. *Inorg. Chem.* **2005**, *44*, 5042-5046. DOI: 10.1021/ic0502832

(35) Toby, B.H.; Von Dreele, R.B. GSAS-II: the genesis of a modern open-source all purpose crystallography software package. *J. Appl. Cryst.* **2013**, *46*, 544-549. DOI: 10.1107/S0021889813003531

(36) Ma, J.; Bo, S.-H.; Wu, L.; Zhu, Y.; Grey, C. P.; Khalifah, P. G. Ordered and Disordered Polymorphs of $Na(Ni_{2/3}Sb_{1/3})O_2$: Honeycomb-Ordered Cathodes for Na-Ion Batteries. *Chem. Mater.* **2015**, 27, 2387−2399. DOI: 10.1021/cm504339y

(37) L. Xiao, Z. Ding, C. Chen, Z. Han, P. Wang, Q. Huang, P. Gao, W. Wei, Insight into the Structural Disorder in Honeycomb-Ordered Sodium-Layered Oxide Cathodes. *iScience*, **2020**, 23, 100898. DOI: 10.1016/j.isci.2020.100898

(38) Shannon, R.D. Revised Effective Ionic Radii and Systematic Studies of Interatomic Distances in Halides and Chalcogenides. *Acta Cryst.* **1976**, *A32*, 751-767. DOI: 10.1107/S0567739476001551

(39) Hempel, F. S.; Sławiński, W. A.; Arstad, B.; Fjellvåg, H. Superstructure of Locally Disordered $Na_2Zn_2TeO_6$, *Chem. Mater*. **2024**, 36, 11084−11094. DOI: 10.1021/acs.chemmater.4c01953

(40) Bain, G. A.; Berry, J. F. Diamagnetic corrections and Pascal's constants. *J. Chem. Educ.* **2008**, 85, 532−236. DOI: 10.1021/ed085p532

(41) Losee, D. B.; McElearney, J. N.; Shankle, G. E.; Carlin, R. L.; Cresswell, P. J.; Robinson, W. T. An Anisotropic Low-Dimensional Ising System, $[(CH_3)_3NH]CoC1_3 \cdot 2H_2O$: Its Structure and Canted Antiferromagnetic Behavior. *Phys. Rev. B*, **1973**, 8, 2185−2199. DOI: 10.1103/PhysRevB.8.2185

(42) Tari, A. The Specific Heat of Matter at Low Temperature (Imperial College Press, London, 2003).

For Table of Contents only

Dilution of Cu^{2+} with non-Jahn-Teller ions eliminates the macroscopic distortion characteristic of monoclinic $Na_2Cu_2TeO_6$ and involves Cu^{2+} into the honeycomb system. Both $Na_2(Co_{2/3}Ni_{2/3}Cu_{2/3})TeO_6$ and $Na_2(Co_{1/2}Ni_{1/2}Cu_{1/2}Zn_{1/2})TeO_6$ order antiferromagnetically at 16.9 and 8.6 K with Weiss temperatures of −38 and −26 K, respectively.

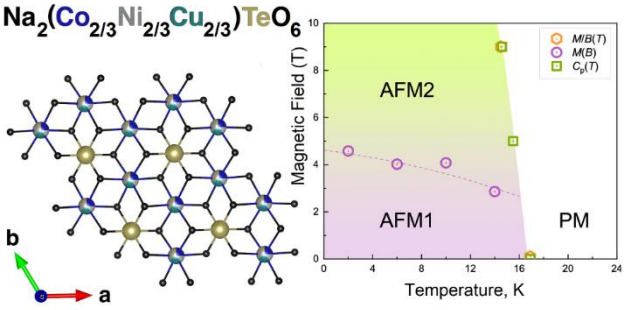

Supporting Information for

Effect of multiple cationic substitutions on structure and magnetism of honeycomb-layered hexagonal tellurates $Na_2M_2TeO_6$ (M = Co, Ni, Cu, Zn)

Vladimir B. Nalbandyan[1,*], Igor L. Shukaev,[1] Maria A. Evstigneeva[1], Alexander N. Vasiliev[2,3], Tatyana M. Vasilchikova[2,3]

[1]*Southern Federal University, Rostov-on-Don 344090, Russia*

[2]*Lomonosov Moscow State University, Moscow 119991, Russia*

S1. Starting materials

All starting materials were of reagent grade. Sodium carbonate was dried at 150 °C, tellurium dioxide, zinc oxide and magnesium oxide were calcined at 400, 500 and 800 °C, respectively, and all of these were stored in a desiccator. Basic carbonates of cobalt, nickel and copper were analyzed by weight loss at 750 °C to give Co_3O_4, NiO and CuO and then used in their air-dry forms.

S2. Sample preparation

Calculated amounts of reagents were weighed to 3-4 decimal places (with 3% Na_2CO_3 excess to compensate for unavoidable soda loss at high temperatures) and mixed carefully with a mortar and pestle. The mixtures were pressed and calcined at 250 °C for an hour to decompose basic carbonates but retain the products in their metastable active forms. After regrinding and pressing, the mixtures were heated slowly in air to 600-650 °C and held at this temperature for 2 hours to start formation of tellurates owing to oxidation of Te(4+) to Te(6+). Then, the pellets were reground, pressed, covered with powders of the same compositions and calcined in covered crucibles, then quenched by dropping the pellets onto a massive steel plate to avoid possible decomposition of the solid solution. For $Na_2(CoNiCu)_{2/3}TeO_6$ this final heat treatment was done at 900 °C for 6 hours. However, it was found later that such harsh conditions are not necessary, and single-phase $Na_2(CoNiCuZn)_{1/2}TeO_6$ was successfully synthetized for 5 h at 850 °C.

S3. Hazards and precautions

Due to volatility and toxicity of tellurium oxides, where tightly closed systems cannot be used, temperatures in the excess of 900 °C should be avoided, the containers should be covered and exhaust ventilation must be provided for the furnace.

*Corresponding author. E-mail: vbn@sfedu.ru

Table S1. Details of structure refinement of $Na_2T_2TeO_6$ (T = $Co_{1/3}Ni_{1/3}Cu_{1/3}$, subcell only, ignoring superstructure reflections) and $Na_2Z_2TeO_6$ (Z = $Co_{1/4}Ni_{1/4}Cu_{1/4}Zn_{1/4}$, true superstructure cell)

M		$Na_{2/3}T_{2/3}Te_{1/3}O_2$	$Na_2Z_2TeO_6$
Crystal system		hexagonal	hexagonal
Space group		*P6₃/mmc* (# 194)	*P6₃22* (# 182)
Lattice parameters, Å	*a*	3.02585(12)	5.25118(10)
	c	11.2139(4)	11.24309(22)
V, Å^3		88.917(7)	268.491(10)
Formula weight		130.12	130.96 × 3
Z		2	2
Wavelength, Å	α_1	1.54056	1.54056
	α_2	1.54439	1.54439
	Ratio	0.5	0.5
No. of points		3901	3851
2Θ range, °		12.00–90.00	13.00–90.00
Step size, °		0.02	0.02
No. of variables		37	49
No. of reflections (α_1 only)			
	calculated	25	67
	observed	25	67
Residuals	$R(F^2)$	0.10816	0.06254
	R_p	0.0586	0.0504
	R_{wp}	0.0770	0.0486
	χ^2	1.820	1.760

Table S2. Atomic coordinates, site occupancy factors and displacement parameters of $Na_2T_2TeO_6$ (T = $Co_{1/3}Ni_{1/3}Cu_{1/3}$, subcell only, ignoring superstructure reflections) and $Na_2Z_2TeO_6$ (Z = $Co_{1/4}Ni_{1/4}Cu_{1/4}Zn_{1/4}$, true superstructure cell)

Atom	Site	*x/a*	*y/b*	*z/c*	SOF	U_{iso}
$Na_2T_2TeO_6$, space group $P6_3/mmc$ for subcell						
$Co_{2/9}Ni_{2/9}Cu_{2/9}Te_{1/3}$	2a	0	0	0		0.0171(6)
Na1	2c	1/3	2/3	1/4	0.460(9)	0.046(8)
Na2	2b	0	0	1/4	0.207(9)	0.078(16)
O	4f	2/3	1/3	0.0928(6)		0.0239(33
$Na_2Z_2TeO_6$, space group $P6_322$ for true supercell						
$Te_{0.804}Ni_{0.196}$	2c	1/3	2/3	1/4		0.0130(7)
$Co_{0.25}Ni_{0.152}Cu_{0.25}Zn_{0.25}Te_{0.098}$	2b	0	0	1/4		0.0234(16)
$Co_{0.25}Ni_{0.152}Cu_{0.25}Zn_{0.25}Te_{0.098}$	2d	1/3	2/3	3/4		0.0247(15)
Na1	6g	0.684(5)	0	0	0.466(6)	0.067(6)
Na2	2a	0	0	0	0	
Na3	4f	1/3	2/3	0.506(4)	0.301(9)	0.072(11)
O	12i	0.3538(15)	0.3366(17)	0.6573(4)		0.0222(22)

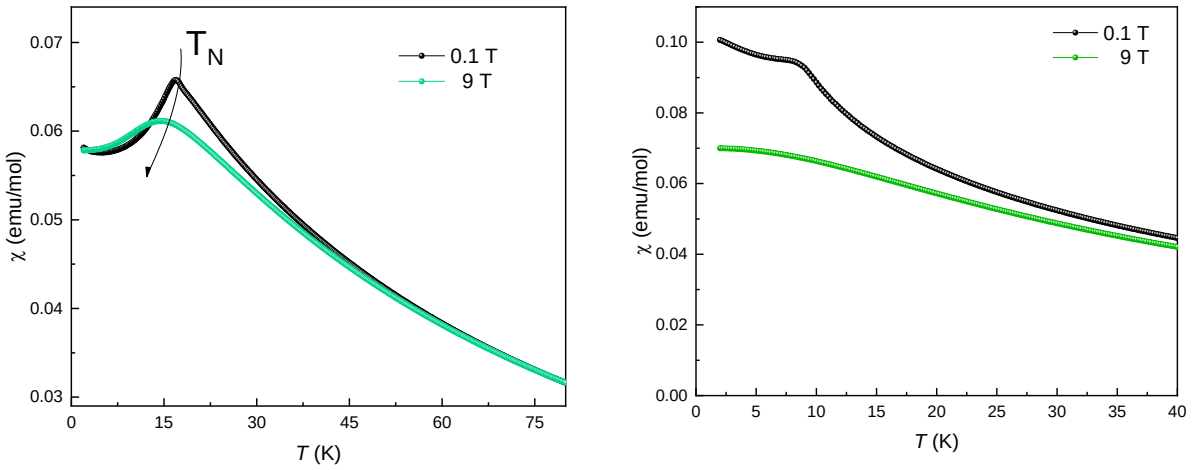

(a) (b)

Fig. S1. Temperature dependencies of magnetic susceptibility M/H(T) at various external magnetic fields for $Na_2T_2TeO_6$ (a) and $Na_2Z_2TeO_6$ (b).

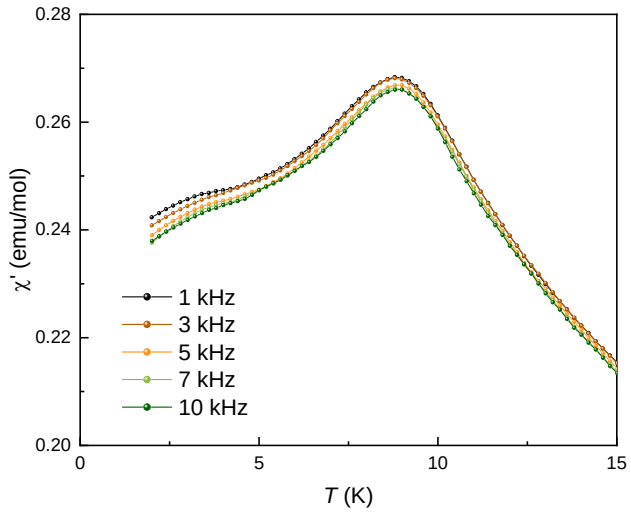

Fig. S2. Temperature dependences of the real χ' part of AC magnetic susceptibility χ_{AC} for $Na_2Z_2TeO_6$

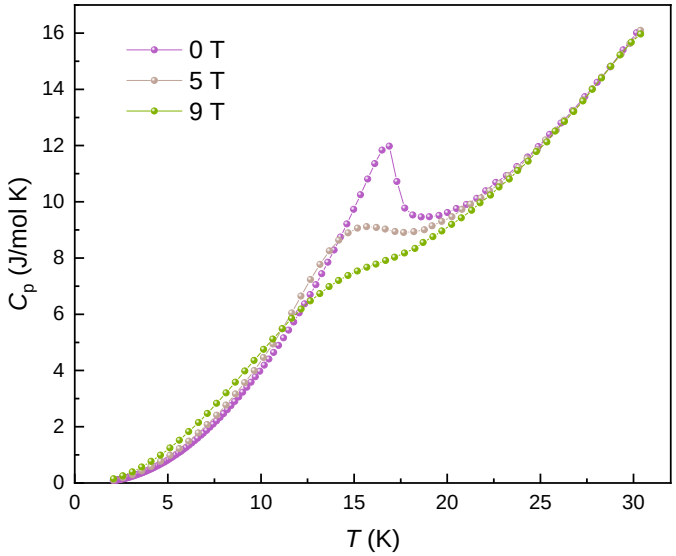

Fig. S3. Temperature dependences of $C_p(T)$ under various magnetic fields for $Na_2T_2TeO_6$.